

# FLOW CONTROL PREDICTIONS USING URANS MODELING: A PARAMETRIC STUDY

**Christopher L. Rumsey**  
NASA Langley Research Center  
Hampton, Virginia 23681, USA  
c.l.rumsey@nasa.gov

**David Greenblatt**  
Institute of Fluid Dynamics and Engineering Acoustics  
8 Mueller-Breslau Street  
Berlin University of Technology, Berlin, Germany  
david.greenblatt@pi.tu-berlin.de

## ABSTRACT

A computational study was performed for steady and oscillatory flow control over a hump model with flow separation to assess how well the steady and unsteady Reynolds-averaged Navier-Stokes equations predict trends due to Reynolds number, control magnitude, and control frequency. As demonstrated previously, the hump model case is useful because it clearly demonstrates a failing in all known turbulence models: they under-predict the turbulent shear stress in the separated region and consequently reattachment occurs too far downstream. In spite of this known failing, three different turbulence models were employed to determine if trends can be captured even though absolute levels are not. The three turbulence models behaved similarly. Overall they showed very similar trends as experiment for steady suction, but only agreed qualitatively with some of the trends for oscillatory control.

## INTRODUCTION

The effective control of flow separation promises substantial performance improvements for a wide variety of air vehicles. Although the methods are well known, there is very little by way of theory or numerical models that can adequately predict lift enhancements, drag reduction, etc. An attempt was made to address this problem by conducting a CFD validation workshop for synthetic jets and turbulent separation control (Rumsey et al. , 2006a) where one case was dedicated to predicting the nominally two-dimensional flow over a hump. The baseline (uncontrolled) case was considered in addition to control by means of steady suction (Greenblatt et al. , 2006a) and zero-net-mass flux (oscillatory) blowing (Greenblatt et al. , 2006b). The workshop determined that CFD with steady or unsteady Reynolds-averaged Navier-Stokes (RANS or URANS) consistently over-predicted the reattachment location, regardless of turbulence model or method. Within the separation bubble, most computations predicted velocity profiles well but considerably under-predicted the magnitude of turbulent shear stresses. Large-eddy simulations and other costly methods appear capable of overcoming this deficiency, but the focus of the current study is on the more affordable RANS and URANS methodologies. See, e.g., Krishnan et al. (2006), Morgan et al. (2006), and Saric et al. (2006).

Although these individual test cases were challenging to CFD codes, only a single test case was considered for both

steady suction and zero-net-mass flux blowing. During the course of the experimental investigation, however, steady and unsteady surface pressures were acquired for a wide variety of control parameters, including Reynolds number, suction flow rate, and frequency and blowing amplitude in the zero-net-mass flux case. By comparing trends of numerical results with experimental data, it should be possible to draw more precise conclusions regarding CFD's value for predictive purposes. Furthermore, a number of important experimental observations were made and it is not known if CFD codes are capable of predicting them. For example, by varying the suction flow rate and comparing these results to high Reynolds number data, the control effectiveness was found to increase substantially with increasing Reynolds number. In addition, for the oscillatory case, the flow was seen to be highly dependent on control frequency and peak blowing amplitude. Different, sometimes counteracting, mechanisms dominated the separated flow-field during different parts of the control cycle. To explore some of these issues, a detailed parametric study using the URANS equations is described here.

## COMPUTATIONAL METHOD

The computer code CFL3D (Krist et al. , 1998) solves the three-dimensional, time-dependent, Reynolds-averaged full Navier-Stokes equations with an upwind finite-volume formulation (it is exercised in two-dimensional mode of operation for the 2-D cases in this study). The Navier-Stokes equations are averaged using Favre averaged variables. Upwind-biased spatial differencing is used for the inviscid terms, and viscous terms are centrally differenced. In time-accurate mode, CFL3D uses pseudo-time stepping with multigrid and achieves second order temporal accuracy. With pseudo-time stepping, subiterations are used to reduce the linearization and factorization errors, and advance the solution to the next physical time.

Three different turbulence models are used in the current study: the Spalart-Allmaras (SA) model (Spalart and Allmaras, 1994), Menter's k-omega SST model (Menter, 1994), and the nonlinear explicit algebraic stress model in k-omega form (EASM-ko) (Rumsey and Gatski, 2003). The turbulence models are implemented uncoupled from the mean-flow Navier-Stokes equations. They are solved using a three-factor implicit approximate factorization approach.

Table 1: Steady suction cases.

$Re \times 10^6$	$c_\mu$ , %	$\dot{m}$ , kg/s
0.5574	0.24	0.0152
0.5574	0.73	0.0263
0.5574	2.59	0.0495
0.936	0.030	0.0053
0.936	0.076	0.0084
*0.936	0.24	0.0152
0.936	0.47	0.0208
0.936	0.73	0.0263
2.0	0.03	0.0053
2.0	0.24	0.0152
2.0	0.47	0.0208
16.0	0.03	0.0053
16.0	0.24	0.0152
16.0	0.47	0.0208
32.0	0.03	0.0053
32.0	0.24	0.0152

## RESULTS

### Flowfield Conditions

The wall-mounted hump model had a chord of  $c = 0.42$  m, height of 0.0538 m at its maximum thickness point, and width of 0.5842 m. The configuration was two-dimensional, and experimental results were demonstrated to be nominally 2-D. The flow control slot was located near 65%  $c$ ; this was close to where the flow separated in its uncontrolled state. A summary of the flowfield conditions studied is provided in Tables 1 and 2. A star appears next to the particular cases used in the workshop in 2004. The Mach number for all computations was  $M = 0.1$ . For the steady suction cases, the steady mass transfer momentum coefficient is defined by:

$$c_\mu = \frac{\rho h U_j^2}{cq} \quad (1)$$

where  $h = 0.00187c$  is the slot height,  $U_j$  is the total jet velocity, and  $q$  is the freestream dynamic pressure. The  $c_\mu$  corresponds with a steady mass flow rate (given by  $\dot{m}$ ) sucked through the slot. For the unsteady oscillatory cases, the oscillatory flow momentum coefficient is defined by:

$$\langle c_\mu \rangle = \frac{\rho h \langle U_j \rangle^2}{cq} \quad (2)$$

where  $\langle U_j \rangle$  is the root-mean-square of the total jet velocity. The  $c_\mu$  and  $\langle c_\mu \rangle$  parameters are typically used in experiments to characterize flow-control blowing levels and are cited as percentages throughout this paper. However, for the purposes of CFD, it is much easier to characterize the levels using  $\dot{m}$  for steady suction and by maximum outflow velocity  $U_{\text{peak}}$  for oscillatory control. Furthermore, for the oscillatory cases, the reduced excitation frequency is defined as  $F^+ = fX/U_\infty$ , where  $X$  is the distance from the slot to flow reattachment point for no flow control. For the purposes of CFD, it is easier to use  $f$ . A great deal of additional information concerning this case can be found on the website for the validation workshop.<sup>1</sup>

<sup>1</sup><http://cfdval2004.larc.nasa.gov>, [cited 3/2007].

Table 2: Unsteady oscillatory control cases.

$Re \times 10^6$	$\langle c_\mu \rangle$ , %	$U_{\text{peak}}$ , m/s	$F^+$	$f$ , Hz
0.936	0.11	27	0.46	83.1
0.936	0.013	8	0.77	138.5
*0.936	0.11	27	0.77	138.5
0.936	0.354	48	0.77	138.5
0.936	0.11	27	1.39	249.3
0.936	0.11	27	2.00	360.1
16.0	0.11	27	0.77	138.5

### Computational Details

The 2-D computations used a fine-level 4-zone grid with 208,320 cells. The jet slot and cavity were included in the hump model computations. Many of the computations used a “medium level” version of the grid consisting of every other point in each coordinate direction, or 52,080 cells. Several grid studies were performed, both here as well as in previous work for the workshop cases (Rumsey, 2006b). These studies indicated that there were almost no differences between mean flow quantities (either long-time-averaged or phase-averaged) on the two grid levels, and less than 5% difference in turbulence quantities. Time step studies were also performed for the oscillatory control case, and indicated that using at least 180 steps per period in conjunction with 20 subiterations per time step was sufficient to yield little perceptible change in results. For all results to be shown here, 360 steps per period were used.

Two different grid families were used, depending on the Reynolds number. Both had the same number of points, but the grid used for  $Re = 16$  and 32 million had a finer minimum spacing at the wall,  $\Delta y/c = 1 \times 10^{-6}$  on the finest level (compared with  $\Delta y/c = 8 \times 10^{-6}$  for the grid used at lower  $Re$ ). On the medium level, this spacing yielded an average minimum  $y^+$  of 1.5 at  $Re = 32$  million, and 0.8 at 16 million, where  $y^+$  represents normal-distance wall units  $y\sqrt{(\tau_w/\rho)/\nu}$ . At lower  $Re$ , the average minimum  $y^+$  was at most 1.1 on the medium level. All grids extended from  $x/c = -6.39$  upstream to 4.0 downstream. The top tunnel wall was included, although the shape was slightly altered to account for blockage caused by the endplates (Rumsey, 2006b). A view of the medium level grid (52,080 cells) used for  $Re$  of 2 million or less is shown in Fig. 1.

The boundary conditions were as follows. At the floor and hump surfaces, as well as at the side walls inside the cavity, solid wall adiabatic boundary conditions were applied. At the front of the grid, a far-field Riemann-type boundary condition was applied. At the downstream boundary the pressure was set to approximately freestream, and all other quantities were extrapolated from the interior of the domain. The top tunnel wall was treated as an inviscid wall for all of the computations shown here. At the bottom of the cavity, the boundary condition for steady suction set the  $u$ -velocity component to 0 and  $v$ -velocity such that the mass flow matched experiment. For the oscillatory cases the velocity components were set with  $u = 0$  and  $v = [(\rho v)_{\text{max}}/\rho] \cos(2\pi ft)$ , where  $f$  is the frequency and  $t$  is the time, and  $(\rho v)_{\text{max}}$  was chosen in order to achieve a maximum outflow velocity magnitude at the exit plane near to the target  $U_{\text{peak}}$  from the experiment.

### Results for Steady Suction

As mentioned in the Introduction, historically all RANS

methods applied to this case have yielded results with too long a separation bubble, because they under-predicted the magnitude of the turbulent shear stress in the separated region. An example is shown in Fig. 2. Here, experimental streamlines for the steady suction case from the workshop are compared with CFD results using SA. In the experiment, the flow reattached near  $x/c = 0.94$ , but in the CFD, the reattachment occurred near  $x/c = 1.1$ . Although not shown, similar results were obtained for other turbulence models.

For the current study, an example of the type of differences generally seen between the three turbulence models tested is given in Fig. 3 for one of the steady suction cases. Here, the SA model gave the best agreement with experiment and EASM-ko the worst, but all three models were reasonably similar to each other. The computed pressures in the region between  $x/c = 0.65$  and 1.2 were all quite different from experiment. This result was consistent with the general finding that the differences between the turbulence models were generally much smaller than the differences between CFD and experiment.

In spite of the fact that we know that CFD using RANS is incapable of obtaining the same quantitative result as experiment in terms of reattachment position, we turn to the question of whether it is capable of predicting trends. Fig. 4 gives surface pressure coefficients at  $Re = 0.936$  million for a range of different  $c_\mu$  coefficients (0.030%, 0.076%, 0.24%, 0.47%, and 0.73%). The CFD exhibited a similar trend as experiment, but the physical details were clearly not correctly modeled. As  $c_\mu$  increased, the separation extent decreased similarly for CFD and experiment, but the CFD predicted pressure drop downstream of the slot instead of a steeper pressure recovery observed in the experiment. The  $c_p$  levels over the forward portion of the hump agreed extremely well with experiment at all  $c_\mu$  conditions.

In the experiment, Greenblatt et al. (2006a) noted a clear Reynolds number effect both at  $c_\mu = 0.24$  and  $c_\mu = 0.47$ , despite the small Reynolds number range tested (from  $Re = 0.557$  million to 1.1 million). Comparisons with a similar hump model (Seifert and Pack, 2002) at a much higher Reynolds number of 16 million showed a continuing Reynolds number effect, which was most evident when comparing form-drag on the respective models (see discussion below). In the CFD results, there was also a clear trend of increasing effectiveness with increasing Reynolds number, as shown in Fig. 5. The largest differences occurred below a  $Re$  of 16 million. This trend is further elucidated in Fig. 6, which summarizes the effect of  $c_\mu$  and  $Re$  on bubble length ( $X_B/c$ ). Here, the general trend of decreasing bubble length with increasing  $c_\mu$  is evident. The only experimental data available were at the lowest  $Re$  of 557,400 and 936,000. The experimental results appeared roughly linear on this log plot. The CFD results were also fairly linear at the lower  $c_\mu$ , but they tended to drop down at the higher  $c_\mu$ . Overall, CFD produced a slightly shallower slope than experiment, along with a significantly longer bubble at the same  $Re$ . The change between  $Re$  of 557,400 and 936,000 was similar for CFD as experiment. The most dramatic shortening of the bubble, as predicted by the CFD, occurred below  $Re = 16$  million; the shortening was small between  $Re = 16$  million and 32 million. Coincidentally, the  $X_B$  levels from CFD at the highest  $Re$  matched fairly well with the experimental levels at the lowest  $Re$ .

Fig. 7 shows the effect of  $c_\mu$  on pressure drag coefficient. Here, experimental results from Seifert and Pack (2002) at a higher Reynolds number of 16 million are also shown. As noted in Greenblatt et al. (2006a), in spite of small geometric

and setup differences that resulted in different baseline  $c_{dp}$  levels, overall there was a clear trend of increasing control effectiveness with increasing  $Re$ . A similar trend was also evident in the CFD results, although the  $c_{dp}$  levels were lower than in the experiments. To better compare the trends, suction results are shown relative to results with no control for  $Re = 0.936$  million in Fig. 8. Here, the computed  $c_{dp}$  trend relative to baseline for all three turbulence models is in good agreement with experiment relative to its baseline, and computed bubble length trend relative to baseline is of correct magnitude but shallower slope than experiment.

## Results for Oscillatory Control

Although streamlines are not shown here, the long-time-averaged bubble size for the oscillatory control case was always over-predicted using RANS. However, as discussed in Rumsey (2006b), the relative motion of the large-scale convected vortical flow structures caused by the pulsed jet/suction were predicted fairly well compared with experiment for the workshop case. Fig. 9 shows comparisons of phase-averaged  $c_p$  at maximum blowing for different  $\langle c_\mu \rangle$  and different  $F^+$ . As for the workshop case, overall the three turbulence models gave results in reasonable qualitative agreement with experiment. However, EASM-ko tended to be less diffusive, maintaining stronger vortices and yielding larger peaks in pressure (particularly for  $F^+ = 0.46$ ).

The effect of Reynolds number on long-time-averaged  $c_p$  is shown in Fig. 10. Here, the experimental results at  $Re = 16$  million were from Seifert and Pack (2002), so small geometric and setup differences may have caused some of the differences in experimental results. Over a smaller Reynolds number range (0.58 million to 1.1 million), Greenblatt et al. (2006b) found no noticeable Reynolds number effect, possibly due to saturation of control authority. Between  $Re = 0.936$  million and 16 million, CFD exhibited a small increase of control effectiveness: the bubble length decreased from  $X_B/c = 0.601$  to 0.536 and  $c_{dp}$  decreased slightly from 0.023 to 0.022. Although not shown, results using SST and EASM-ko were qualitatively similar to SA.

The effect of  $\langle c_\mu \rangle$  on  $c_p$  is shown in Fig. 11. The experiment showed a lowering of the pressure downstream of the slot, accompanied by a shortening of the bubble with increasing  $\langle c_\mu \rangle$ , but the CFD exhibited almost no difference at all at the two lowest blowing conditions tested. Because of this, a higher blowing velocity not corresponding with any experiment was run ( $U_{peak} = 63$  m/s) in order to better establish the trend in the CFD. (This condition is not listed in Table 2 because the precise oscillatory momentum coefficient corresponding to  $U_{peak} = 63$  m/s is not known; however, it is estimated to be near  $\langle c_\mu \rangle \approx 0.65$ .) With this additional run included, it is clear that CFD followed a similar trend as experiment at the higher blowing coefficients. The experiment also indicated that the flowfield “saturated” in terms of giving its most negative minimum  $c_p$  in the separated region when  $\langle c_\mu \rangle = 0.11\%$ . In the CFD, there was also a pressure drop in the bubble, but it was more gradual than the experiment and minimum  $c_p$  occurred for both  $\langle c_\mu \rangle = 0.013\%$  and 0.11%. Then higher  $\langle c_\mu \rangle$  produced higher pressure levels in the bubble. Although not shown, results using SST and EASM-ko exhibited similar trends to SA.

The effect of  $F^+$  on  $c_p$  is shown in Fig. 12. In the experiment, increasing  $F^+$  produced slightly smaller separation bubbles up to  $F^+$  near 1.39, but then the trend reversed at higher  $F^+$ . In the CFD, no such trend was seen. Instead, if anything, the bubble lengths increased slightly with in-

creasing  $F^+$ , but the differences were generally very small. Another noticeable trend in the CFD (not seen in the experiment) was a pronounced peak in the minimum bubble pressure at  $F^+ = 0.46$ , and higher minimum levels at higher  $F^+$ . Although not shown, this peak was even more pronounced for the SST and EASM-ko results.

Finally, Fig. 13 shows  $c_{dp}$  as a function of  $\langle c_\mu \rangle$  for two different  $F^+$  using all three turbulence models. As with the steady suction case, the CFD under-predicted the absolute  $c_{dp}$  levels, but the general trend of relatively flat  $c_{dp}$  for  $\langle c_\mu \rangle < 0.11$  appears to be similar to experiment. (Compare this plot with Fig. 7, which indicates a negative slope over all of the  $c_\mu$  range.) In the experiment, this apparent ineffectiveness at low  $\langle c_\mu \rangle$  was due to offsetting effects of shortening bubble and increasing pressure drop immediately downstream of the slot, but in the CFD the trend was due to the fact that  $\langle c_\mu \rangle$  had little effect on the average pressure distribution. At higher  $F^+$ , the CFD predicted lower  $c_{dp}$  (like experiment), but the difference was nearly half that seen in the experiment. The three turbulence models differed by as much as 17%, with SST predicting the highest drag levels and SA the lowest.

## SUMMARY AND CONCLUSIONS

An extensive computational study was conducted with RANS and URANS and three different turbulence models in application to the hump model case from a flow control validation workshop held in 2004. Many of these cases were not part of the workshop itself, but were included in the experiment. They included investigations into the effects of Reynolds number, control magnitude, and control frequency, and have not been computed before. The purpose of this study was to investigate the effectiveness of RANS and URANS CFD for predicting trends in this type of flow control application.

In summary, all three turbulence models performed similarly, in the sense that differences between the models were generally much less than differences between CFD and experiment, although the SA model was slightly superior to the others. For steady suction, CFD appeared capable of qualitatively predicting the effects of Reynolds number and  $c_\mu$ , and this was clearly evident by comparing bubble length and form-drag changes. Nevertheless, the pressure recovery details were not correctly predicted. The fact that both experiment and CFD showed a strong  $Re$  effect is important because the majority of experiments are performed at low Reynolds number laboratory conditions ( $Re \leq 1,000,000$ ) and are assumed to remain valid under typical flight conditions with  $Re$  at several tens of millions.

For oscillatory control, the CFD indicated increasing effectiveness in the mean with increasing  $Re$ , but the effect was not nearly as pronounced as with steady suction. This was consistent with the data of Greenblatt et al (2006b), but at odds with that of Seifert and Pack (2002) and therefore no firm conclusions could be drawn. CFD did not appear to mimic the mean effect of increasing oscillatory momentum coefficient very well. In particular, at levels less than about  $\langle c_\mu \rangle = 0.35$ , CFD results showed little improvement over no flow control at all. At  $\langle c_\mu \rangle > 0.35$ , CFD started to show pronounced influence due to higher amplitude blowing/suction. Some effects due to changes in control frequency were captured qualitatively by CFD in the phase-averaged results, but trends in the mean (long-time-averaged surface pressures) were missed.

## REFERENCES

- Greenblatt, D., Paschal, K. B., Yao, C.-S., Harris, J., Schaeffler, N. W., and Washburn, A. E., 2006a, "Experimental Investigation of Separation Control Part 1: Baseline and Steady Suction," *AIAA Journal*, Vol. 44, No. 12, pp. 2820–2830.
- Greenblatt, D., Paschal, K. B., Yao, C.-S., and Harris, J., 2006b, "Experimental Investigation of Separation Control Part 2: Zero Mass-Efflux Oscillatory Blowing," *AIAA Journal*, Vol. 44, No. 12, pp. 2831–2845.
- Krishnan, V., Squires, K. D., Forsythe, J. R., 2006, "Prediction of Separated Flow Characteristics over a Hump," *AIAA Journal*, Vol. 44, No. 2, pp. 252–262.
- Krist, S. L., Biedron, R. T., and Rumsey, C. L., 1998, "CFL3D User's Manual (Version 5.0)," NASA TM-1998-208444.
- Menter, F. R., 1994, "Two-Equation Eddy-Viscosity Turbulence Models for Engineering Applications," *AIAA Journal*, Vol. 32, No. 8, pp. 1598–1605.
- Morgan, P. E., Rizzetta, D. P., Visbal, M. R., 2006, "High-Order Numerical Simulation of Turbulent Flow over a Wall-Mounted Hump," *AIAA Journal*, Vol. 44, No. 2, pp. 239–251.
- Rumsey, C. L. and Gatski, T. B., 2003, "Summary of EASM Turbulence Models in CFL3D with Validation Test Cases," NASA/TM-2003-212431.
- Rumsey, C., Gatski, T., Sellers, W., Vatsa, V., and Viken, S., 2006a, "Summary of the 2004 Computational Fluid Dynamics Validation Workshop on Synthetic Jets," *AIAA Journal*, Vol. 44, No. 2, pp. 194–207.
- Rumsey, C., 2006b, "Reynolds-Averaged Navier-Stokes Analysis of Zero Efflux Flow Control over a Hump Model," AIAA Paper 2006-1114.
- Saric, S., Jakirlic, S., Djugum, A., Tropea, C., 2006, "Computational Analysis of a Locally Forced Flow over a Wall-Mounted Hump at High-Re Number," *Int. Journal of Heat and Fluid Flow*, Vol. 27, No. 4, pp. 707–720.
- Seifert, A., and Pack, L. G., 2002, "Active Flow Separation Control on Wall-Mounted Hump at High Reynolds Numbers," *AIAA Journal*, Vol. 40, No. 7, pp. 1363–1372.
- Spalart, P. R., and Allmaras, S. R., 1994, "A One-Equation Turbulence Model for Aerodynamic Flows," *La Recherche Aeronautique*, No. 1, pp. 5–21; also AIAA Paper 92-0439, 1992.

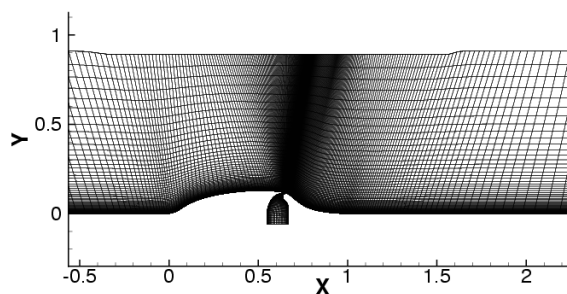


Figure 1: View of medium-level grid (52,080 cells).

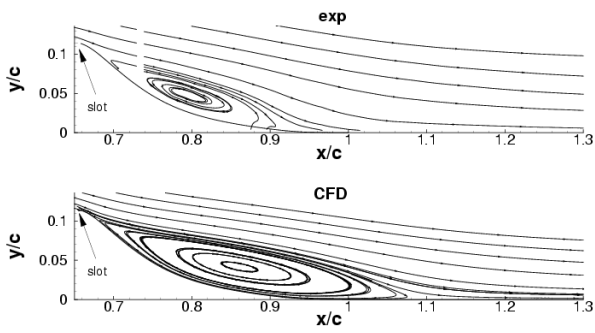


Figure 2: Streamlines for steady suction case,  $Re = 0.936$  million,  $c_\mu = 0.24$ ; CFD shows results using SA model.

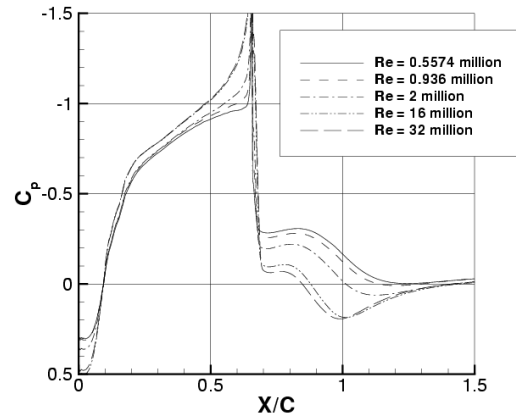


Figure 5: Effect of Reynolds number on surface pressure coefficients for steady suction,  $c_\mu = 0.24$ ; CFD only, showing results using SA model.

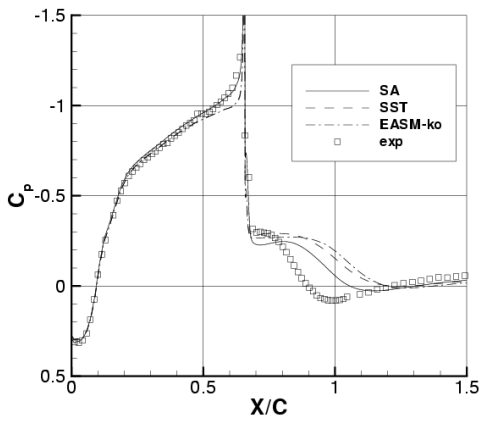


Figure 3: Surface pressure coefficients for steady suction case,  $Re = 0.936$  million,  $c_\mu = 0.47$ .

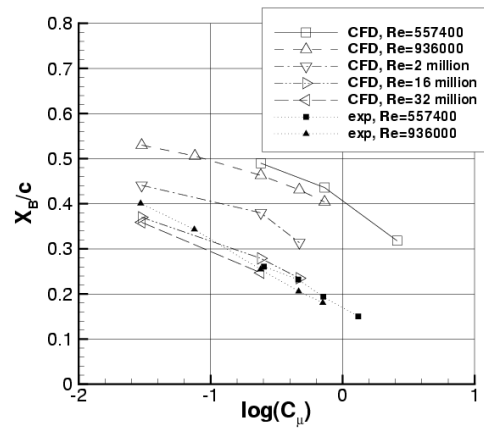


Figure 6: Bubble length as a function of  $c_\mu$  for steady suction; CFD shows results using SA model.

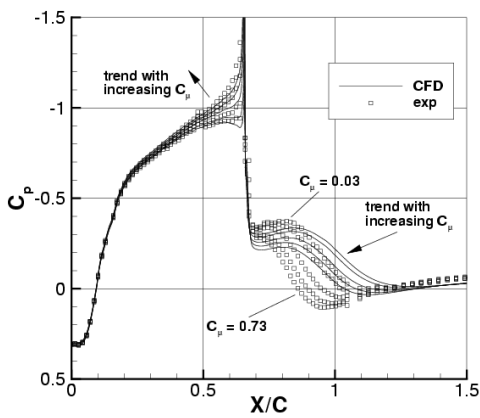


Figure 4: Effect of  $c_\mu$  on surface pressure coefficients for steady suction,  $Re = 0.936$  million; CFD shows results using SA model.

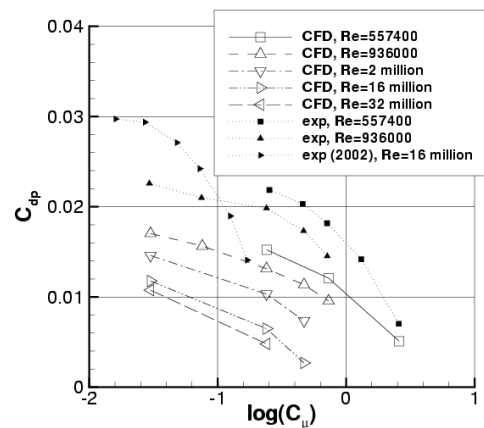


Figure 7: Pressure drag coefficient as a function of  $c_\mu$  for steady suction; CFD shows results using SA model.

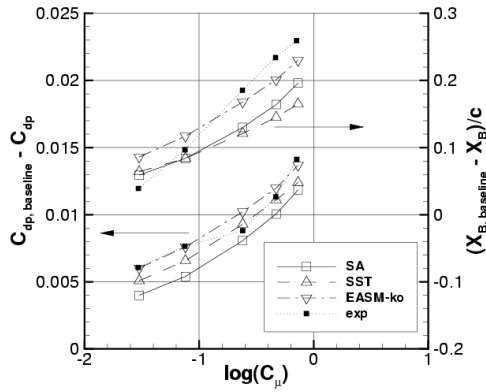


Figure 8: Bubble length and pressure drag coefficient relative to baseline (no control) as a function of  $c_\mu$  for steady suction,  $Re = 0.936$  million.

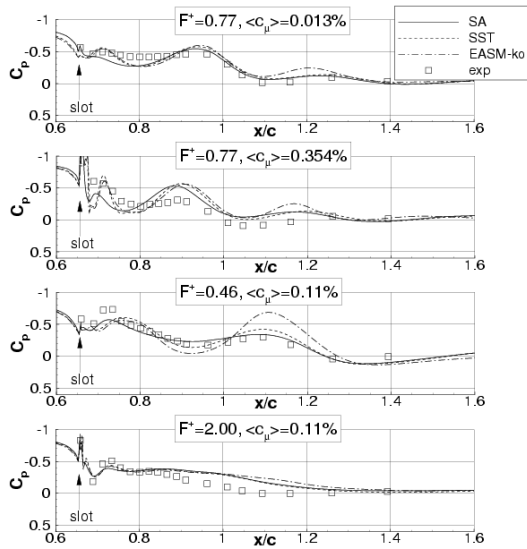


Figure 9: Phase-averaged surface pressure coefficients behind the hump at maximum blowing phase of the cycle for oscillatory control;  $Re = 0.936$  million.

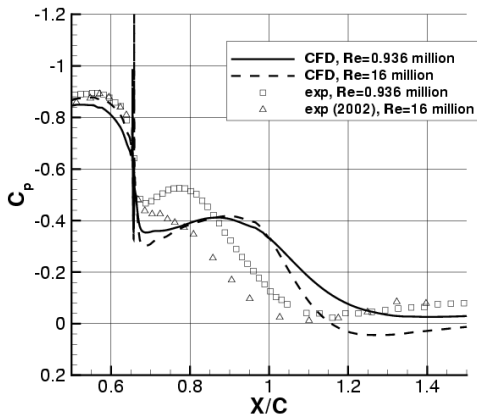


Figure 10: Effect of Reynolds number on long-time-averaged surface pressure coefficients for oscillatory control;  $\langle c_\mu \rangle = 0.11\%$ ,  $F^+ = 0.77$ ; CFD shows results using SA model.

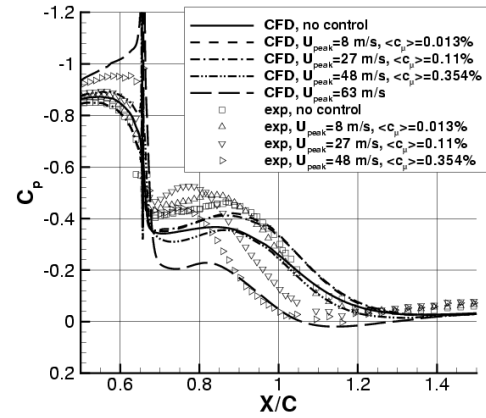


Figure 11: Effect of  $\langle c_\mu \rangle$  on long-time-averaged surface pressure coefficients for oscillatory control;  $Re = 0.936$  million,  $F^+ = 0.77$ ; CFD shows results using SA model.

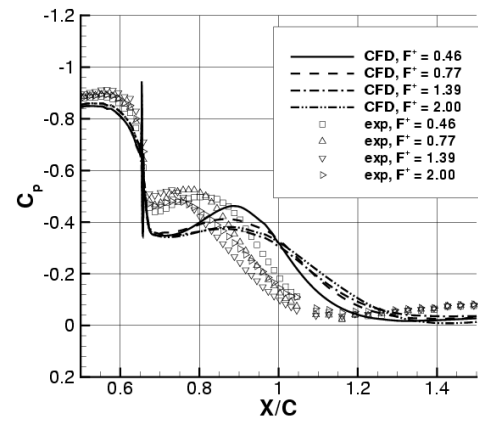


Figure 12: Effect of  $F^+$  on long-time-averaged surface pressure coefficients for oscillatory control;  $Re = 0.936$  million,  $\langle c_\mu \rangle = 0.11\%$ ; CFD shows results using SA model.

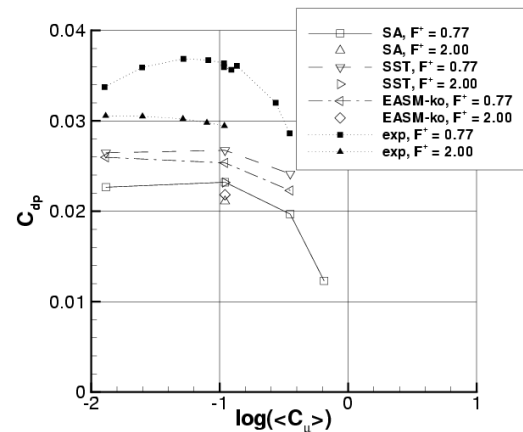


Figure 13: Pressure drag coefficient as a function of  $\langle c_\mu \rangle$  for oscillatory control;  $Re = 0.936$  million.